Chem-Bio Informatics Journal, Vol.23, pp.14–25 (2023)

Application of Model Core Potentials to Zn- and Mg-containing Metalloproteins in the Fragment Molecular Orbital Method

Koichiro Kato*[1, 2], Ami Yamamoto[3], Chiduru Watanabe[4, 5], Kaori Fukuzawa[3, 6]

[1] Department of applied chemistry, Graduate School of Engineering, Kyushu University, 744 Motooka, Noshi-ku, Fukuoka 819-0395 Japan
[2] Center for Molecular System, Kyushu University, 744 Motooka, Noshi-ku, Fukuoka 819-0395 Japan
[3] Department of Physical Chemistry, School of Pharmacy and Pharmaceutical Sciences, Hoshi University, 2-4-41 Ebara, Shinagawa-ku, Tokyo 142-8501, Japan
[4] Center for Biosystems Dynamics Research, RIKEN, 1-7-22 Suehiro-cho, Tsurumi-ku, Yokohama, Kanagawa 230-0045, Japan
[5]JST PRESTO, 4-1-8, Honcho, Kawaguchi, Saitama 332-0012, Japan
[6]Graduate School of Pharmaceutical Sciences, Osaka University, 1-6 Yamadaoka, Suita, Osaka 565-0871, Japan

**E-mail: kato.koichiro.957@m.kyushu-u.ac.jp*

(Received February 28, 2023; accepted June 15, 2023; published online July 20, 2023)

Abstract

The fragment molecular orbital (FMO) method enables quantum mechanical calculations for macromolecules by dividing the target into fragments. However, most calculations, even for metalloproteins, have been performed by removing metal ions from the structures registered in the Protein Data Bank (PDB). For more realistic and useful calculations, FMO calculations must be performed without removing the metal ions. In this study, we discuss the results obtained from FMO calculations performed using 6-31G* and model core potentials (MCPs) for metal proteins containing Zn and Mg ions. Subsequently, we analyze the differences in atomic charges and interactions.

Key Words: FMO calculation; PIEDA; Atomic charge; Fragmentation; Zn^{2+} ions; Mg^{2+} ions, Model Core Potential

Area of Interest: Molecular recognition and molecular modeling

Licensed under a Creative Commons Attribution 4.0 International (CC BY 4.0)

1. Construction of a protein structure and conditions of FMO calculations

In order to properly treat metalloprotein in fragment molecular orbital (FMO) calculations, we investigated the application with/without the model core potentials (MCPs)[1,2] to metal ions in SARS-CoV-2 helicase (PDBID:7NN0)[3]. Helicases are important proteins that unwind double-stranded DNA into single strands. We have previously performed 60 calculations on helicase [4] and 60 results using auto-FMO protocol have been published in the FMODB (https://drugdesign.riken.jp/FMODB/)[5,6]; however, the calculations were performed with all metal ions removed. Therefore, in this study, FMO calculations were performed without removing the three Zn ions and one Mg ion contained in the complex between SARS-CoV-2 helicase and a phosphoaminophosphonic acid-adenylate ester (ANP). For basis functions, in addition to the standard 6-31G*, we used MCPs[1,2] with a fixed number of inner-shell electrons for metal atoms. Subsequently, the atomic charges[7] and pair interaction energy decomposition analyses (PIEDA)[8,9] of each metal ion were compared.

Structural preprocessing was performed for the SARS-CoV-2-related proteins in a previous study[4]. The helicase complex was obtained by X-ray crystallographic data with a resolution of 3.04 Å (PDBID: 7NN0). The protein structure is shown in Figure 1. First, the complexes were prepared using “Structural Preparation” and “Protonate 3D” functions in the Molecular Operating Environment (MOE, v2020.09; Chemical Computing Group Inc., Montreal, QC, Canada), where missing atoms completion and hydrogen addition were also performed. Structural optimization was performed using AMBER10:EHT force field, where the restraint condition was that all heavy atoms were constrained with a tether weight (1.0 kcal/Å) and all hydrogen atoms unconstrained. The resulting structure is shown in Figure 1.

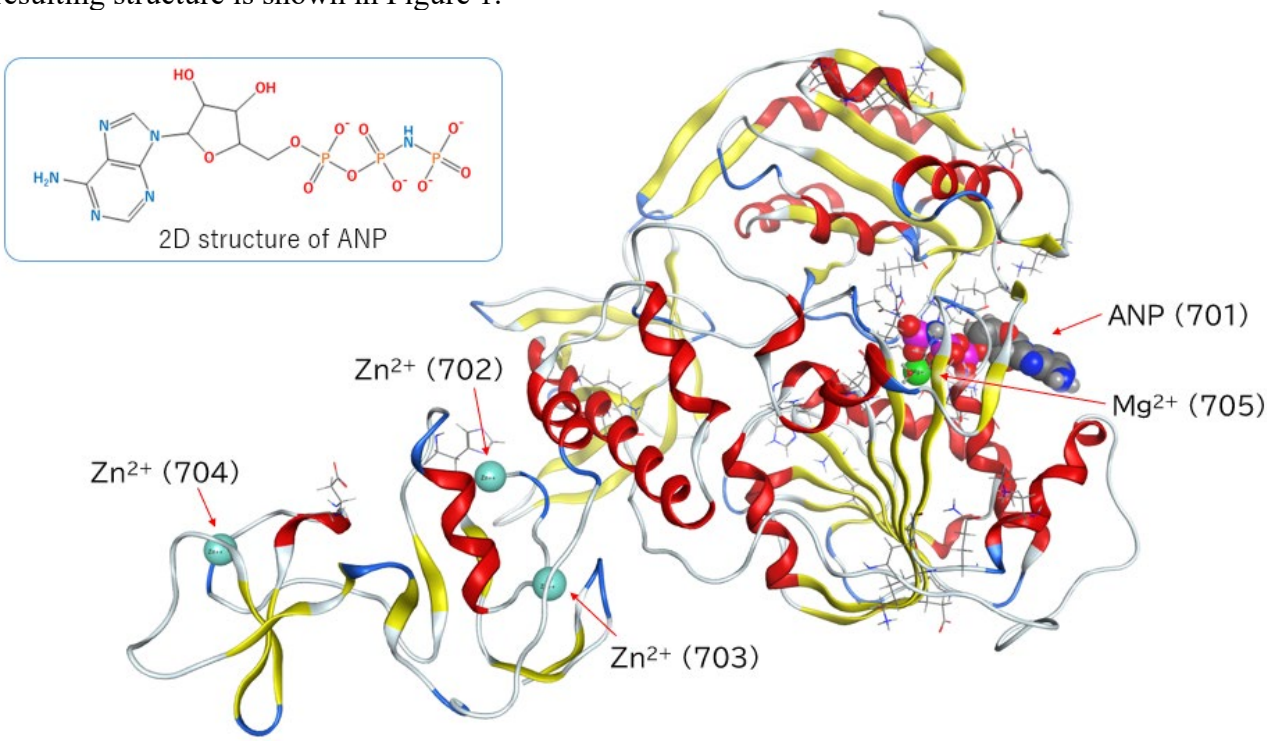

Figure 1. Structure of the SARS-CoV-2 Helicase and ANP complex including Zn^{2+} and Mg^{2+} ions (PDBID:7NN0)

The fragmentation was the same as that in the conventional FMO calculation, i.e., amino acid unit fragmentation. However, there were three Zn^{2+} ions and one Mg^{2+} ion in the PDB entry 7NN0. Considering the coordination bonds, the fragments around the four metal ions were reconstructed as shown in Figure 2. ZN702 contains two histidine residues (HIS33 and HIS39) and two coordinated cysteine residues (CYS16 and CYS19). The side chains of these four amino acid residues and ZN702 merged to form a single fragment (Figure 2(a)). Similarly, ZN703 and the side chains of CYS5, CYS8, CYS26, and CYS29 combined to form a single fragment (Figure 2(b)). ZN704 combined with the side chains of CYS50, CYS55, CYS72, and HIS75 to form a single fragment (Figure 2(c)). MG705 is adjacent to the 3-phosphate portion of the ligand ANP701 and three H_2O molecules. After fragmenting ANP701 at the 3-phosphate moiety, MG701, 3-phosphate, and three H_2O molecules combined to form a single fragment (Fig. 2(d)). As an example of the fragmentation scheme with bond detached atoms (BDAs) and bond attached atoms (BAAs), the constructions of fragments around ZN702 are shown in Figure 3.

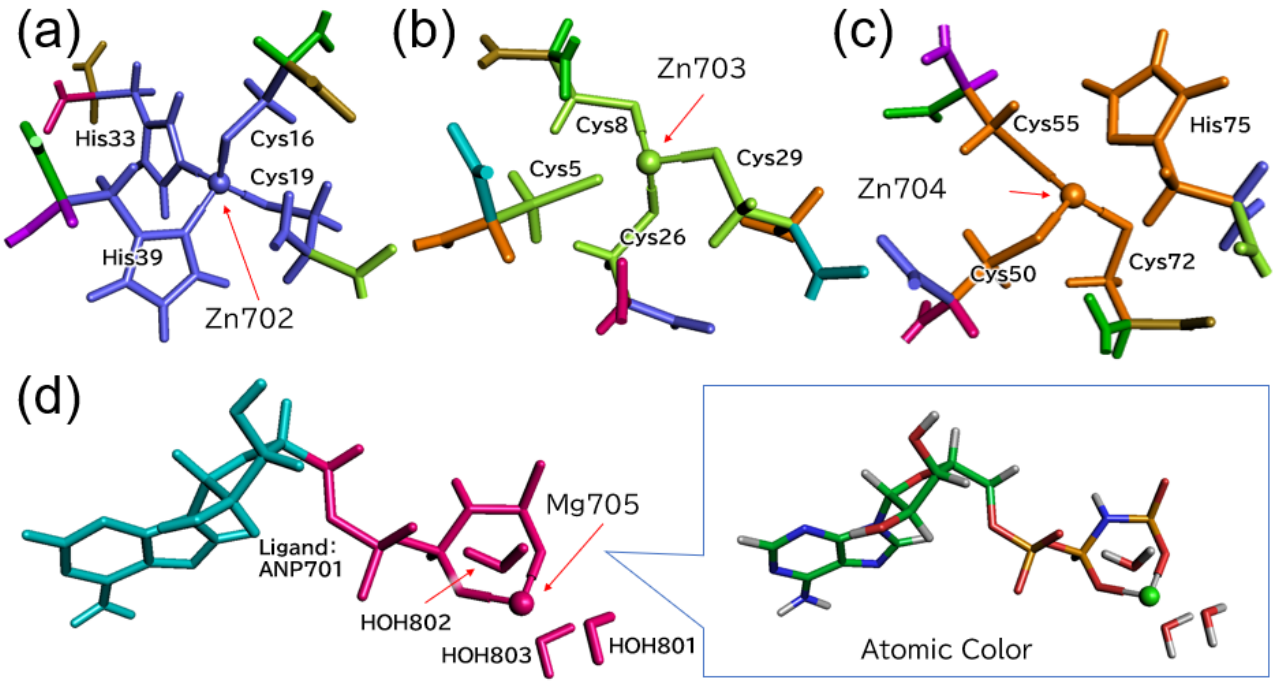

Figure 2. Fragmentation around (a) ZN702, (b) ZN703, (c) ZN704, and (d) MG705. Atoms of the same color belong to the same fragment

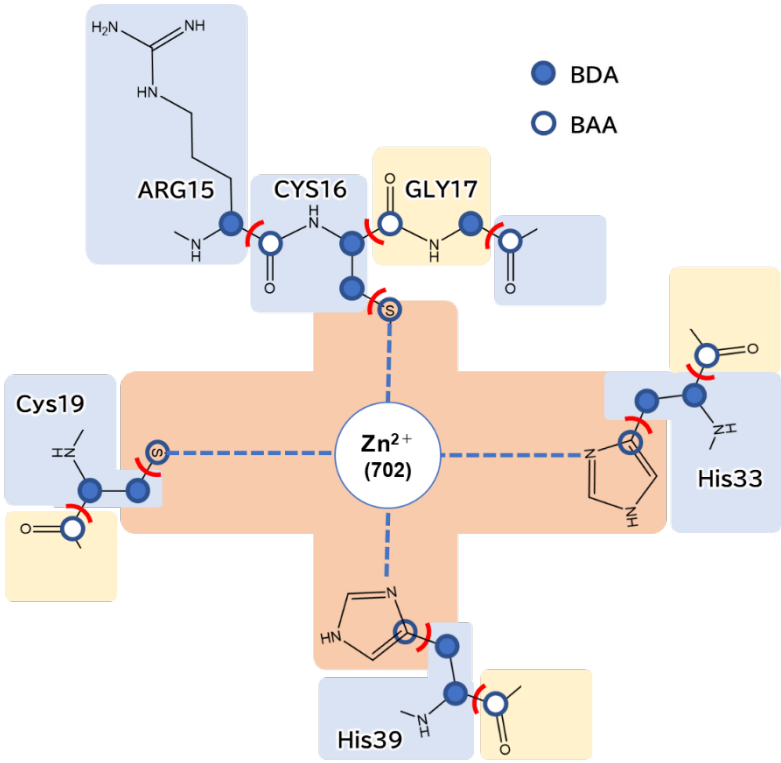

Figure 3. Fragmentation around Zn^{2+} (702) with clearly stated BDA and BAA

FMO calculations were performed using ABINIT-MP, an application for quantum chemical calculations based on the fragment molecular orbital (FMO) method[10,11]. Based on FMO calculation at MP2/6-31G* level, two patterns of metal treatment were investigated: (1) metal ions were also applied to 6-31G*, and (2) MCPs were only applied to metal ions. The MCPs were used to read a file downloaded from ref. 12. In ABINIT-MP, multiple downloaded MCP files of Zn^{2+} and Mg^{2+} ions can be merged into a single file, and the MCPs can be applied to specific elements by specifying it in the input file, as shown in Figure 4. The format of the MCP file to be loaded into ABINIT-MP is described in the user manual. All calculations were performed on a "Fugaku" supercomputer at RIKEN. The FMO data of the complex with and without MCPs has been registered in the FMODB with the codes (FMODB ID) as 43QQN and Q8Q1Y, respectively.

```
&MCP
 CHKMCP='YES'
 TYPE='READ'
 NELEM=2
 ELEM='12,30'
 ReadMCP='mcp.dat'
/
```

Figure 4. Specifying MCPs in ABINIT-MP input file

2. Results of FMO calculations

The natural bond orbital (NBO) charges for each metal ion, calculated for 6-31G* and MCPs, are listed in Table 1. The coordination bond lengths of each metal ion and its surrounding fragments are shown in Table 2. The average atomic charge of the three Zn^{2+} ions was 1.558 *e* for 6-31G* and 1.923 *e* for the MCPs. In contrast, for the Mg^{2+} ions, the atomic charge was 1.662 *e* for 6-31G* and 1.995 *e* for MCP. For both metal ions, there was more electron influx from the surrounding fragments in 6-31G* than in the MCPs, moving them from a positively charged state closer to a neutral charge. These results were obtained because the MCPs replace the inner-shell electrons with a model nucleus, which suppresses charge transfer, unlike 6-31G*. Among all the metal ions, Zn^{2+} (703) showed the largest charge transfer, with a change of 0.525 *e* for 6-31G* and 0.108 *e* for MCPs.

Table 1. Natural bond orbital charges for each metal ion in 6-31G* and MCPs

Metal Ion (Residue number)	Natural bond orbital charge [*e*]	
	All 6-31G*	MCP
Zn^{2+} (702)	1.650	1.953
Zn^{2+} (703)	1.475	1.892
Zn^{2+} (704)	1.549	1.924
Mg^{2+} (705)	1.662	1.995

Table 2. Coordination bond lengths between each metal ion and its surrounding fragments

Metal Ion (Residue number)		Distance （Å）
Zn^{2+} (702)	SG (CYS16)	1.921
	SG (CYS19)	1.914
	ND1 (His36)	1.931
	ND1 (His39)	1.939
Zn^{2+} (703)	SG (CYS5)	2.012
	SG (CYS8)	1.968
	SG (CYS26)	1.983
	SG (CYS29)	1.959
Zn^{2+} (704)	SG (CYS50)	1.959
	SG (CYS55)	1,930
	SG (CYS72)	1.957
	ND1 (HIS75)	2.050
Mg^{2+} (705)	O1G (ANP701)	1.786
	O2B (ANP701)	1.897
	O (HOH801)	2.025
	O (HOH803)	2.023

Because atomic charge transfer can cause changes in interactions, we analyzed the total inter-fragment interaction energy (IFIE) and conducted PIEDA for fragments containing a metal ion. The interaction energies of Zn^{2+} (702) fragment with each amino acid residue of the helicase are listed in Table 3, where differences of IFIEs between 6-31G* and MCP greater than ±0.2 kcal/mol are enumerated. The most significant change is in the interaction with Zn^{2+}(702), with a difference of −1.1 kcal/mol. A change in the interaction was also observed for the charged amino acids ARG22 and ARG21. This was attributed to changes in the ES associated with atomic charge transfer. In Table 3, there are neutrally charged amino acids with a total IFIE greater than 100 kcal/mol between them

and Zn^{2+}(702). These include LYS40, GLY17, and ILE20. As shown in Figure 2(a), these are fragments neighboring the amino acids (HIS39, CYS16, and CYS19) that merge with Zn^{2+}(702). This combination with Zn^{2+}(702) was only performed for the side chains, and the main-chain moiety was a small independent fragment. The interaction between this small fragment with BDA and fragments with BAA (LYS40, GLY17, and ILE20; Figure 3) was significantly large, but this may be an artifact of fragmentation. Although it is not shown in Table 3, due to the small difference between 6-31G* and MCP, VAL34 is also similar to the three fragments above, with an IFIE of 133.0 kcal/mol with Zn^{2+}(702). In ordinary fragmentation, the interactions between fragments involving the splitting of covalent bonds are not considered[12,13]. These results suggest that when metal ions are treated through special fragmentation, as in this study, their interactions with the fragments in the second neighbor to fragments containing a metal ion must be ignored. Here, the second neighbor fragment is a sequence behind one of the amino acid residues whose side chain is coordinated to the metal ion and an amino acid residue covalently bonded to the residue (Figure 3). The 3D structure around Zn702, including Arg21, Arg22, Val34, and Lys40, is shown in Figure 5. The results for the other fragments containing a metal ion are listed in Tables 4–6, and the values of fragments that should be ignored are shown in parentheses. Differences were observed in the interactions of each metal ion with other metal ions and charged amino acid residues. These changes are reasonable given the change in the atomic charges of the metal ions.

Table 3. Total IFIE and PIEDA of Zn^{2+} ion (702) fragment with each amino acid residue of the helicase

ES, EX, CT+mix, and DI in the table represent electrostatic, exchange repulsion, charge transfer, and dispersion interactions, respectively. The upper half represents each value calculated by 6-31G*. The lower half shows the results of each value calculated with 6-31G* minus those calculated with MCP. IFIEs with a difference between 6-31G* and MCP greater than ±0.2 kcal/mol were enumerated. Numbers with () are values that should be ignored (see text).

6-31G*	IFIE [kcal/mol]	PIEDA [kcal/mol]				Charge transfer [*e*]		Distance [Å] †
Fragment	Total	ES	EX	CT+mix	DI	q(I->J)	Main	
ZN2703	1.4	1.4	0.0	0.0	0.0	0.000	ES	4.59
ARG22	-12.3	-11.3	0.4	-0.6	-0.9	0.000	ES	2.76
ARG21	-8.6	-7.7	0.3	-0.5	-0.7	-0.003	ES	2.57
VAL42	6.7	7.7	0.1	-0.3	-0.9	0.002	ES	4.25
PHE24	0.7	1.0	0.0	0.0	-0.2	0.000	ES	4.06
ASP32	-6.7	-6.4	0.0	-0.2	-0.1	0.000	ES	4.65
CYS30	-4.2	-2.2	2.3	-2.1	-2.2	0.016	EX	2.65
ASP59	0.4	0.4	0.0	0.0	0.0	0.000	ES	8.60
ASN107	-20.2	-21.7	8.8	-3.9	-3.5	0.050	ES	1.81
PRO23	-5.3	-5.2	5.5	-2.6	-3.0	0.003	EX	4.59
ILE35	0.4	0.7	0.0	-0.1	-0.2	0.000	ES	2.08
LYS28	0.5	0.5	0.0	0.0	0.0	0.000	ES	4.21
ASP113	-2.9	-2.9	0.0	0.0	0.0	0.000	ES	7.60
VAL34	133.0	23.0	19.9	94.5	-4.5	0.101	CT+mix	7.22
LEU43	-2.2	-2.2	0.0	0.0	0.0	0.000	ES	1.54
LYS40	143.7	27.6	16.5	102.2	-2.5	0.116	CT+mix	5.83
ARG15	-7.7	-7.3	0.0	-0.1	-0.3	0.000	ES	1.54
THR111	-14.7	-10.7	2.3	-2.4	-3.9	0.024	ES	4.63
ALA110	0.9	1.8	4.7	-2.3	-3.2	0.003	EX	2.57
GLY17	(131.7)	(19.6)	(20.2)	(98.2)	(-6.4)	(0.143)	CT+mix	2.46
ILE20	(140.5)	(15.7)	(21.5)	(104.6)	(-1.4)	(0.093)	CT+mix	1.53

Difference in each value of the MCP data from the 6-31G* data

Fragment	Total	ES	EX	CT+mix	DI	q(I->J)
ZN2703	-1.1	-1.1	0.0	0.0	0.0	0.000
ARG22	-0.8	-1.0	0.0	0.1	0.1	0.000
ARG21	-0.8	-0.7	0.0	0.0	0.0	0.000
VAL42	-0.7	-0.5	0.0	0.0	-0.2	0.000
PHE24	-0.4	-0.4	0.0	0.0	0.0	0.000
ASP32	-0.4	-0.4	0.0	0.0	0.0	0.000
CYS30	-0.4	-0.3	0.0	0.0	-0.1	0.000
ASP59	-0.2	-0.2	0.0	0.0	0.0	0.000
ASN107	-0.2	-0.2	0.0	0.0	0.0	0.001
PRO23	0.2	-0.2	0.2	0.3	-0.1	0.000
ILE35	0.2	0.2	0.0	0.0	0.0	0.000
LYS28	0.3	0.3	0.0	0.0	0.0	0.000
ASP113	0.3	0.3	0.0	0.0	0.0	0.000
VAL34	0.3	0.3	0.0	0.0	-0.1	0.001
LEU43	0.3	0.3	0.0	0.0	0.0	0.000
LYS40	0.4	0.1	-0.1	0.2	0.1	0.002
ARG15	0.4	0.4	0.0	0.0	0.1	0.000
THR111	0.5	0.3	0.0	0.2	0.0	0.001
ALA110	0.8	0.1	0.3	0.6	-0.1	0.001
GLY17	(1.9)	(2.0)	(1.3)	(-1.0)	(-0.4)	(0.005)
ILE20	(4.4)	(-4.5)	(-0.3)	(6.2)	(2.9)	(-0.003)

† Distance between nearest neighbor atoms of a fragment pair.

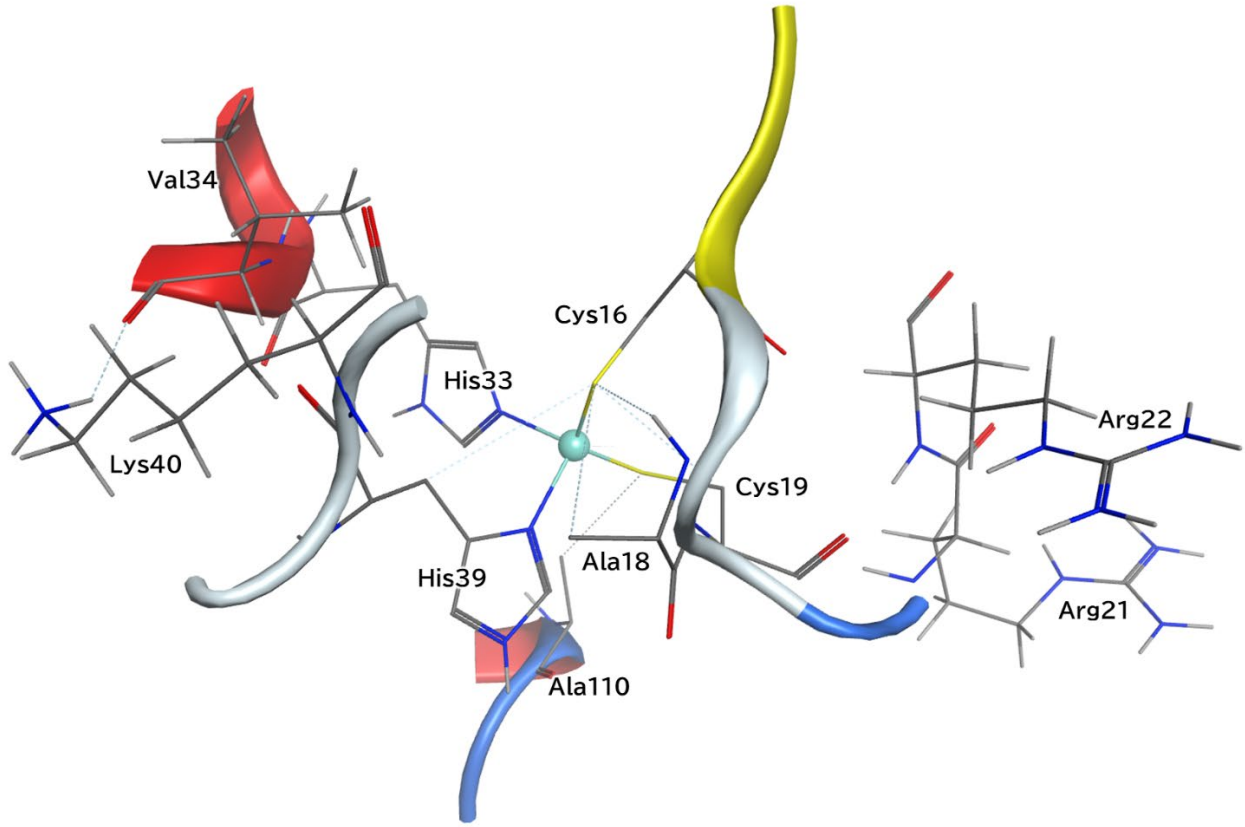

Figure 5. 3D structure diagram around Zn702 showing the positions of the amino acids, in particular Arg21, Arg22, Val34, and Lys40

Table 4. Total IFIE and PIEDA of Zn^{2+} ion (703) fragment with each amino acid residue of the helicase

ES, EX, CT+mix, and DI in the table represent electrostatic, exchange repulsion, charge transfer, and dispersion interactions, respectively. The upper half represents each value calculated by 6-31G*. The lower half shows the results of each value calculated with 6-31G* minus those calculated with MCP IFIEs with a difference between 6-31G* and MCP greater than ±0.2 kcal/mol were enumerated. Numbers with () are values that should be ignored (see text).

6-31G*	IFIE [kcal/mol]	PIEDA [kcal/mol]				Charge transfer [*e*]		Distance [Å] †
Fragment	total	ES	EX	CT+mix	DI	q(I->J)	Main	
ZN1702	1.4	1.4	0.0	0.0	0.0	0.000	ES	4.59
GLY99	-22.5	-23.7	9.7	-5.1	-3.5	0.004	ES	2.57
GLN11	5.0	5.5	1.6	-0.9	-1.2	0.009	ES	2.74
LYS28	(-104.8)	(-102.0)	(2.2)	(-2.2)	(-2.9)	-0.013	ES	3.15
GLU136	38.6	38.6	0.0	0.0	0.0	0.000	ES	13.67
THR12	6.8	8.5	0.6	-0.8	-1.4	0.005	ES	3.03
VAL98	-15.1	-13.3	0.7	-0.9	-1.7	-0.002	ES	2.55
PHE24	-1.8	-1.6	0.0	0.0	-0.2	0.000	ES	4.75
LEU25	5.3	7.1	4.7	-2.9	-3.6	0.003	ES	2.15
VAL2	-46.0	-46.0	0.0	0.0	0.0	0.000	ES	8.95
CYS97	1.2	-11.4	29.2	-10.6	-6.0	-0.052	EX	1.99
ASP101	57.5	57.5	0.0	0.0	0.0	0.001	ES	4.68
ARG129	-60.6	-60.6	0.0	0.0	0.0	0.000	ES	7.11
ASP32	71.8	72.3	0.0	-0.1	-0.4	0.000	ES	4.78
VAL6	(118.8)	(12.1)	(19.4)	(93.1)	(-5.8)	0.117	CT+mix	1.54
SER10	-11.0	-11.0	12.5	-6.8	-5.6	-0.002	EX	1.75
ASN9	(105.3)	(-4.0)	(21.0)	(94.6)	(-6.1)	0.082	CT+mix	1.54
LEU7	-22.9	-23.1	16.2	-8.1	-7.9	0.014	ES	2.41
CYS27	(120.8)	(3.2)	(21.0)	(102.0)	(-5.4)	0.107	CT+mix	1.53
Difference in each value of the MCP data from the 6-31G* data								
Fragment	**total**	**ES**	**EX**	**CT+mix**	**DI**	**q(I->J)**		
ZN1702	-1.1	-1.1	0.0	0.0	0.0	0.000		
GLY99	-1.0	-1.7	1.4	-0.5	-0.1	0.012		
GLN11	-0.9	-0.8	0.0	0.0	-0.1	0.000		
LYS28	(-0.7)	(-1.7)	(0.7)	(0.3)	(0.0)	(0.006		
GLU136	-0.2	-0.2	0.0	0.0	0.0	0.000		
THR12	0.2	0.1	0.0	0.0	0.0	0.000		
VAL98	0.3	-0.2	0.1	0.4	0.0	0.002		
PHE24	0.3	0.2	0.0	0.0	0.0	0.000		
LEU25	0.3	-0.4	0.7	0.2	-0.2	0.008		
VAL2	0.4	0.4	0.0	0.0	0.0	0.000		
CYS97	0.4	-1.3	2.0	-0.4	0.2	0.009		
ASP101	0.5	0.2	0.0	0.3	0.0	0.001		
ARG129	0.6	0.6	0.0	0.0	0.0	0.000		
ASP32	0.7	0.7	0.0	0.0	0.0	0.000		
VAL6	(0.9)	(1.5)	(0.4)	(-0.7)	(-0.3)	(0.004)		
SER10	1.2	0.7	-0.1	0.6	0.0	0.000		
ASN9	(1.3	(-0.1	(-0.2	(1.6	(0.1	-0.001		
LEU7	2.0	-0.3	2.9	-0.7	0.2	0.019		
CYS27	(2.3)	(-0.9)	(1.1)	(1.5)	(0.6)	(0.000)		

† Distance between nearest neighbor atoms of a fragment pair.

Table 5. Total IFIE and PIEDA of Zn^{2+} ion (704) fragment with each amino acid residue of the helicase

ES, EX, CT+mix, and DI in the table represent electrostatic, exchange repulsion, charge transfer, and dispersion interactions, respectively. The upper half represents each value calculated by 6-31G*. The lower half shows the results of each value calculated with 6-31G* minus those calculated with MCP. IFIEs with a difference between 6-31G* and MCP greater than ±0.2 kcal/mol were enumerated. Numbers with () are values that should be ignored (see text).

6-31G*	IFIE (kcal/mol)	PIEDA [kcal/mol]				Charge transfer [*e*]		Distance [Å] †
Fragment	**total**	**ES**	**EX**	**CT+mix**	**DI**	**q(I->J)**	**Main**	
LYS76	(96.3)	(-17.4)	(16.3)	(100.1)	(-2.8)	(0.090)	CT+mix	1.54
THR58	-3.7	-2.8	0.2	-0.3	-0.8	0.005	ES	3.20
TYR64	-8.9	-8.7	0.0	0.0	-0.2	0.000	ES	5.31
GLY54	-2.1	-1.7	0.0	-0.1	-0.3	0.000	ES	4.48
ASP59	26.3	26.3	0.0	0.0	0.0	0.000	ES	6.05
TYR70	-2.9	-2.9	0.0	0.0	0.0	0.000	ES	5.87
VAL49	-1.0	-0.4	0.0	-0.2	-0.4	0.000	ES	3.69
PRO53	-2.4	-2.1	0.4	0.3	-1.0	0.005	ES	3.10
TYR71	0.8	1.2	5.4	-2.4	-3.4	-0.004	EX	2.80
LEU63	4.8	5.7	0.8	-0.5	-1.3	0.000	ES	2.63
ASP56	(180.9)	(66.0)	(22.0)	(98.7)	(-5.8)	(0.134)	CT+mix	1.53
ASN51	(121.0)	(8.0)	(19.3)	(98.4)	(-4.6)	(0.115)	CT+mix	1.54
ALA52	-15.1	-15.9	15.6	-7.6	-7.3	-0.006	ES	2.18
LYS73	(92.0)	(-27.8)	(20.4)	(104.1)	(-4.8)	(0.104)	CT+mix	1.53
Difference in each value of the MCP data from the 6-31G* data								
Fragment	**total**	**ES**	**EX**	**CT+mix**	**DI**	**q(I->J)**		
LYS76	(-0.5)	(-0.9)	(-0.1)	(0.4)	(0.1)	(0.001)		
THR58	-0.5	-0.7	0.0	0.3	-0.1	0.001		
TYR64	-0.2	-0.2	0.0	0.0	0.0	0.000		
GLY54	0.2	0.1	0.0	0.0	0.1	0.000		
ASP59	0.3	0.3	0.0	0.0	0.0	0.000		
TYR70	0.3	0.3	0.0	0.0	0.0	0.000		
VAL49	0.3	0.2	0.0	0.0	0.0	0.000		
PRO53	0.5	-0.1	0.0	0.5	0.1	0.001		
TYR71	0.5	-0.6	1.0	0.5	-0.4	0.004		
LEU63	0.7	0.5	0.0	0.2	0.0	0.000		
ASP56	(0.9)	(0.7)	(0.0)	(0.3)	(-0.1)	(0.001		
ASN51	(1.1)	(1.1)	(0.7)	(-0.9)	(0.2)	0.001		
ALA52	2.2	0.9	1.8	-0.5	0.1	-0.002		
LYS73	(2.8)	(-3.1)	(0.6)	(4.0)	(1.3)	(0.001		

† Distance between nearest neighbor atoms of a fragment pair.

Table 6. Total IFIE and PIEDA of Mg^{2+} ion (705) fragment with each amino acid residue of the helicase

ES, EX, CT+mix, and DI in the table represent electrostatic, exchange repulsion, charge transfer, and dispersion interactions, respectively. The upper half represents each value calculated by 6-31G*. The lower half shows the results of each value calculated with 6-31G* minus those calculated with MCP. IFIEs with a difference between 6-31G* and MCP greater than ±0.2 kcal/mol were enumerated. Numbers with () are values that should be ignored (see text).

6-31G*	IFIE [kcal/mol]	PIEDA [kcal/mol]				Charge transfer [*e*]		Distance [Å] †
Fragment	**total**	**ES**	**EX**	**CT+mix**	**DI**	**q(I->J)**	**Main**	
ASP374	0.3	4.0	27.2	-18.9	-12.0	0.244	EX	1.62
SER289	-53.6	-79.0	49.7	-18.2	-6.1	0.024	ES	1.96
GLU375	30.6	13.1	43.1	-17.2	-8.5	0.149	EX	1.59
SER539	-8.2	-16.7	13.2	-0.8	-3.7	0.054	ES	1.72
GLU540	102.3	103.0	2.3	-1.3	-1.7	0.017	ES	2.46
ASP401	85.7	86.0	0.0	0.0	-0.3	0.000	ES	4.60
ALA316	0.3	1.0	0.0	-0.2	-0.5	0.002	ES	3.21
GLY287	-21.9	-22.6	8.1	-3.5	-3.9	-0.023	ES	2.29
GLN404	-13.1	-16.6	9.7	-3.1	-3.2	-0.039	ES	1.85
LYS569	-59.5	-59.5	0.0	0.0	0.0	0.000	ES	6.25
THR286	-7.9	-14.4	1.8	7.2	-2.5	0.009	ES	2.36
ARG442	-67.0	-66.8	0.0	0.0	-0.2	0.000	ES	3.59
LYS465	-58.7	-58.7	0.0	0.0	0.0	0.000	ES	7.34
LYS320	-153.2	-156.3	13.7	-5.2	-5.4	-0.068	ES	2.19
GLY285	-27.4	-33.0	18.2	-6.3	-6.3	-0.043	ES	1.70
GLY538	-12.3	-11.2	5.5	-4.3	-2.4	-0.028	ES	2.62
ARG567	-144.3	-158.4	27.1	-7.0	-5.9	-0.082	ES	1.74
HIS290	-11.8	-17.7	11.5	-2.5	-3.1	-0.019	ES	1.89
ARG443	-196.7	-213.8	43.8	-14.0	-12.7	-0.104	ES	1.70
Difference in each value of the MCP data from the 6-31G* data								
Fragment	**total**	**ES**	**EX**	**CT+mix**	**DI**	**q(I->J)**		
ASP374	-9.0	1.4	0.4	-5.7	-5.0	0.117		
SER289	-5.5	-11.4	9.2	-6.9	3.6	0.013		
GLU375	-2.6	-0.9	0.1	-0.8	-1.0	0.012		
SER539	-0.8	-0.8	-0.1	0.3	-0.8	0.004		
GLU540	-0.8	-0.7	0.0	0.0	-0.1	0.000		
ASP401	-0.3	-0.3	0.0	0.0	-0.1	0.000		
ALA316	-0.3	0.0	0.0	0.0	-0.2	0.001		
GLY287	0.2	0.3	0.0	0.0	-0.1	0.001		
GLN404	0.2	0.2	0.0	0.0	0.0	0.001		
LYS569	0.2	0.2	0.0	0.0	0.0	0.000		
THR286	0.2	0.3	0.0	-0.1	0.0	0.000		
ARG442	0.3	0.2	0.0	0.0	0.0	0.000		
LYS465	0.3	0.3	0.0	0.0	0.0	0.000		
LYS320	0.3	0.1	0.1	0.1	0.1	0.004		
GLY285	0.4	0.4	0.0	0.0	-0.1	0.002		
GLY538	0.4	-0.1	1.1	-0.9	0.4	-0.004		
ARG567	1.1	1.0	0.0	0.0	0.0	0.003		
HIS290	1.6	-1.0	-0.1	1.1	1.7	0.018		
ARG443	2.0	1.6	0.3	-0.1	0.2	0.003		

† Distance between nearest neighbor atoms of a fragment pair.

The computation time for 6-31G* was 10590.3 s (approximately 3 h), using 48 nodes of "Fugaku" at RIKEN, whereas that of the MCPs was 10572.6 s, using the same computing resources; thus, there was no significant difference in the computation times between them.

As mentioned above, the MCPs works in the direction of suppressing atomic charge transfers. Therefore, we also attempted a calculation in which fragmentation was performed as usual and all metal ions were treated as independent fragments. However, the calculations did not converge in either the 6-31G* or MCPs case. Because the calculation of fragment dimers containing Zn^{2+} ions that form coordination bonds did not converge, the coordination bonds should be merged to form a single fragment, as in this paper, rather than fragmenting the coordination bonds.

3. Conclusion

We performed FMO calculations for the SARS-CoV-2 helicase and ANP complex including Zn^{2+} and Mg^{2+} ions (PDBID: 7NN0) using 6-31G* and MCP basis functions for metal ions. Then the difference in the atomic charge of the metal ions between the isolated and complex forms was milder with the MCPs. MCP seems to be more consistent with chemically intuition, since the atomic charges are closer to the valence of the ions, but it is difficult to determine which is more desirable. Results also revealed that the difference in the interaction energies with the change in the atomic charge due to 6-31G* and MCP basis functions was generally less than 1 kcal/mol and was not affect the qualitative discussion of interfragment interactions.

Acknowledgements

This study was conducted as a part of the FMO Drug Design Consortium (FMODD). We thank Professor Yuji Mochizuki of Rikkyo University and Drs. Tatsuya Nakano and Yoshio Okiyama of the National Institute of Health Sciences for providing the Fugaku version of ABINIT-MP and for general discussions on the FMO calculations. We also thank Drs. Teruki Honma, Daisuke Takaya, and Kikuko Kamisaka at RIKEN for their helpful comments and technical assistance regarding FMODB registration. The FMO calculations were performed using Fugaku (Project ID: hp220143) at RIKEN. This work was supported in part by the Japan Agency for Medical Research and Development (AMED) under the Drug Discovery and Life Science Research Support Platform Project (BINDS) (Grant No. JP22ama121030). CW acknowledges the JST PRESTO Research Grant (JPMJPR18GD).

References

[1] Miyoshi, E.; Mori, H.; Hirayama, R.; Osanai, Y.; Noro, T.; *et al*. Compact and Efficient Basis Sets of S- and p-Block Elements for Model Core Potential Method. *J. Chem. Phys.* **2005**, *122* (7), 074104. https://doi.org/10.1063/1.1845392

[2] Ishikawa, T.; Mochizuki, Y.; Nakano, T.; Amari, S.; Mori, H.; *et al*. Fragment Molecular Orbital Calculations on Large Scale Systems Containing Heavy Metal Atom. *Chem. Phys. Lett.* **2006**, *427* (1), 159–165. https://doi.org/10.1016/j.cplett.2006.06.103

[3] Newman, J. A.; Douangamath, A.; Yadzani, S.; Yosaatmadja, Y.; Aimon, A.; *et al.* Structure, Mechanism and Crystallographic Fragment Screening of the SARS-CoV-2 NSP13 Helicase. *Nat. Commun.* **2021**, *12* (1), 4848. https://doi.org/10.1038/s41467-021-25166-6

[4] Fukuzawa, K.; Kato, K.; Watanabe, C.; Kawashima, Y.; Handa, Y.; *et al*. Special Features of COVID-19 in the FMODB: Fragment Molecular Orbital Calculations and Interaction Energy Analysis of SARS-CoV-2-Related Proteins. *J. Chem. Inf. Model.* **2021**, *61* (9), 4594–4612. https://doi.org/10.1021/acs.jcim.1c00694

[5] Watanabe, C.; Watanabe, H.; Okiyama, Y.; Takaya, D.; Fukuzawa, K.; *et al*. Development of an Automated Fragment Molecular Orbital (FMO) Calculation Protocol toward Construction of Quantum Mechanical Calculation Database for Large Biomolecules. *Chem-Bio Inform. J.* **2019**, *19*, 5–18. https://doi.org/10.1273/cbij.19.5

[6] Takaya, D.; Watanabe, C.; Nagase, S.; Kamisaka, K.; Okiyama, Y.; *et al*. FMODB: The World's First Database of Quantum Mechanical Calculations for Biomacromolecules Based on the Fragment Molecular Orbital Method. *J. Chem. Inf. Model.* **2021**, *61* (2), 777–794. https://doi.org/10.1021/acs.jcim.0c01062

[7] Reed, A. E.; Weinstock, R. B.; Weinhold, F. Natural Population Analysis. *J. Chem. Phys.* **1985**, *83* (2), 735–746. https://doi.org/10.1063/1.449486

[8] Fedorov, D. G.; Kitaura, K. Pair Interaction Energy Decomposition Analysis. *J. Comput. Chem.* **2007**, *28* (1), 222–237. https://doi.org/10.1002/jcc.20496

[9] Tsukamoto T.; Kato K.; Kato A.; Nakano T.; Mochizuki Y.; *et al*. Implementation of Pair Interaction Energy DecompositionAnalysis and Its Applications to Protein-Ligand Systems. *J. Comput. Chem. Jpn.* **2015**, *14* (1), 1–9. https://doi.org/10.2477/jccj.2014-0039

[10] Tanaka, S.; Mochizuki, Y.; Komeiji, Y.; Okiyama, Y.; Fukuzawa, K. Electron-Correlated Fragment-Molecular-Orbital Calculations for Biomolecular and Nano Systems. *Phys. Chem. Chem. Phys.* **2014**, *16* (22), 10310–10344. https://doi.org/10.1039/C4CP00316K.

[11] *Recent Advances of the Fragment Molecular Orbital Method*; Mochizuki, Y., Tanaka, S., Fukuzawa, K., Eds.; Springer, 2021.

[12] Watanabe, C.; Fukuzawa, K.; Okiyama, Y.; Tsukamoto, T.; Kato, A.; *et al*. Three- and Four-Body Corrected Fragment Molecular Orbital Calculations with a Novel Subdividing Fragmentation Method Applicable to Structure-Based Drug Design. *J. Mol. Graph. Model.* **2013**, *41*, 31–42. https://doi.org/10.1016/j.jmgm.2013.01.006

[13] Fukuzawa, K.; Watanabe, C.; Okiyama, Y.; Nakano, T. How to Perform FMO Calculation in Drug Discovery. In *Recent Advances of the Fragment Molecular Orbital Method: Enhanced Performance and Applicability*; Mochizuki, Y., Tanaka, S., Fukuzawa, K., Eds.; Springer: Singapore, 2021; pp 93–125. https://doi.org/10.1007/978-981-15-9235-5_7